Accurate estimation for the closed-loop robust control using global modes

Gilles Tissot, Jean-Pierre Raymond

Institut de Mathématiques de Toulouse, UMR CNRS 5219, Université Paul Sabatier, 31062 Toulouse, France.

Résumé :

L'utilisation de modes globaux pour la stabilisation des écoulements oscillateurs est parfaitement adaptée, car cette modélisation prend en compte la partie instable de la dynamique linéaire responsable de la croissance modale des perturbations. Ce sous-espace instable est de petite dimension, et la plupart du temps suffisant pour obtenir un contrôle efficace. Cependant, lorsque l'on considère un estimateur, la modélisation de la partie stable de grande dimension est nécessaire afin d'assurer la compatibilité entre la mesure et son estimation. La partie stable, est classiquement approximée par projection de Galekin. Dans ce contexte, la troncature équilibrée ou la BPOD (balanced POD) sont souvent préférés à la sélection de modes globaux, principalement pour leur capacité à approximer les comportements entrée/sortie. Dans ce papier, nous nous affranchissons de l'approximation due à l'étape de projection et nous modélisons l'effet de la partie stable sur l'observation par un terme intégral, dont le noyaux de convolution est de faible dimension. Cette méthode garantie la stabilité du système compensé et améliore ses performances $\mathcal{H}_\infty$. De plus, nous discutons de l'ajout de modes stables afin d'améliorer l'estimation dans une optique de contrôle robuste. L'équation de Ginzburg-Landau est considérée dans ce papier comme un modèle simplifié ayant un comportement similaire à celui des écoulements.

Abstract:

The control using global modes is well suited for the feedback stabilization of oscillatory fluid systems, since it takes into account the unstable dynamics responsible of perturbations growth. The unstable subspace is of small dimension and, most of the time, sufficient to obtain good control performances. But, when an estimator is considered, modeling the high-dimensional stable part is required to ensure consistency between measurement and estimation. The stable part is classically approximated by Galerkin projection onto a well suited basis. Balanced truncation modes or balanced POD are often preferred to global mode's selection, mainly for their ability to approximate input-output behaviors. In this paper, we avoid the Galerkin approximation and we model the effect of the stable part in the observation by an integral term whose associated kernel is of small dimension and easy to pre-compute. This method guarantees the stability of the compensated system and improves its $\mathcal{H}_\infty$ performance. Moreover, we give some guidelines to select additional stable modes to enhance estimation in a robust control perspective. The Ginzburg-Landau equation is used as a model problem having a behavior similar than that of fluid flows.

Key words: Robust control, Global modes, Estimation, Ginzburg-Landau equation, Mode's selection.

1 Introduction

In this paper, we are interested in performing an observer-based state feedback stabilization of the Ginzburg-Landau equation. This equation is often considered as a good surrogate model for fluid flows. One particular constraint, in fluid systems, is the high number of degrees of freedom involved in the system dynamics. In the design process, modeling the intrinsic hydrodynamic instability allows to define low-order controllers, that, at moderate Reynolds numbers, can stabilize the flow with a minimal actuation cost (Raymond and Thevenet, 2010). To be able to act in real-time, the computation time to update the control needs to be smaller than the characteristic time of the flow. The low dimension of the controller is then mandatory in practical applications. Moreover, the full state of the system is rarely known, but only some measurements, submitted to a certain level of noise, are available. Estimation of the reduced-order state may become a delicate task since consistency between the measurement and the low-order model is not guaranteed. Indeed, the measure does not distinguish the contribution of the part involved in the reduced-order model from the neglected part. Projection-based reduced-order methods, with various choices of basis, are then classically employed for minimizing the observation error. It is first clear that the finite number of unstable modes, if they exist, need to be modeled, since they drive the oscillatory behavior of the flow. For an accurate estimation, the infinite dimensional stable part needs to be incorporated in some way (Sipp and Schmid, 2016). Adding a finite (even large) set of eigenmodes have demonstrated poor performances (Barbagallo et al., 2009; Ehrenstein et al., 2011; Barbagallo et al., 2011) and even sometimes a loss of stability of the compensated system. This failure has been understood to be caused, among other things, by the non-normality of the considered basis and its lack of input-output representativeness. Modeling the stable part can also be expressed with other bases such as POD modes (Lumley, 1967), balanced truncation (BT, Antoulas and Sorensen, 2001) or balanced POD (BPOD, Rowley, 2005). These bases have the advantage of controlling the projection error and then to ensure a reduction of the observation inconsistency. Unfortunately, due to the truncation the linear dynamics is corrupted, leading to two disadvantages that render uncertain the compensated system performances: *i)* the optimality associated with the computation of the controller and Kalman gain is lost, *ii)* the estimator dynamics is corrupted. Thus, we need to add a number of modes large enough so that the error bound between the reduced order model and the system is sufficiently small to guarantee the stability and the expected performances.

In this paper, we propose an alternative approach to model the stable part of the system, in the Kalman filter, by an integral term coming from the underlying linear dynamics of the full stable part excited by the actuation. An associated low-dimensional kernel can be pre-computed at a reasonable cost even for large scale systems. The structure of the proposed compensator guarantees stability of the compensated system.

In a second step, additional stable global modes can be incorporated in the model, that allows us to take into account the response of the stable part to external perturbations and thus to enhance the estimation. We give some guidelines for mode's selection in that context, in a perspective of robustness improvement of the control law.

The Ginzburg-Landau equation is used in this paper to demonstrate the necessity of having a special care of the estimation. This equation is widely used for modeling typical features of non-parallel fluid flows (Roussopoulos and Monkewitz, 1996), and it is commonly employed as a benchmark control problem (Bagheri et al., 2009; Chen and Rowley, 2011).

In section 2 we present the Ginzburg-Landau equation, the method used to obtain a discretized model

and to build a low-order controller and estimator. In section 3 we compare different ways of coupling the plant and the compensator. Numerical tests are used to highlight the necessity of introducing an integral term in the Kalman filter. Finally, in section 4, we discuss how to introduce some stable modes explicitly in the estimator to enhance estimation and robustness.

2 Problem formulation

2.1 Ginzburg-Landau equation

We consider the control of the complex Ginzburg-Landau equation for $\psi(x,t) \in \mathbb{C}$, with $x \in \Gamma = (0,\ell)$, $t \in (0,T)$:

$$\begin{cases} \dfrac{\partial \psi}{\partial t} + U\dfrac{\partial \psi}{\partial x} = \mu(x)\psi + \nu\dfrac{\partial^2 \psi}{\partial x^2} + c_d(x,t) + f_d(x,t) \\ \psi(0,t) = c_b(t), \quad \dfrac{\partial \psi}{\partial x}(\ell,t) = 0, \quad \psi(x,0) = 0. \end{cases} \tag{1}$$

The domain size is $\ell = 150$ and the time horizon $T = 500$. The control parameters are a distributed control $c_d(x,t)$ null outside an actuation region $\Gamma_c = [60, 100]$ and a non-homogeneous Dirichlet boundary condition $c_b(t)$. Here, the perturbation $f_d(x,t)$ is a Gaussian white noise distributed in Γ, of variance σ_f^2 with $\sigma_f = 10^{-3}$. We also define some sensor measurements of ψ: y_1 localized at $x_{o1} = 47$, maximum amplification position and $y_2(x)$ distributed over $\Gamma_o = [90, 130]$. Sensors are perturbed as well by Gaussian white noises, of variance σ_o^2 with $\sigma_o = 10^{-3}$. Our parameter selection is inspired from Lauga and Bewley (2003): $U = 6$, $\nu = 1 - 10i$, $\mu(x) = \mu_0 - (\xi(x - x_t))^2$ with $\mu_0 = 1.4\mu_a$, $\mu_a = U^2\text{real}(\nu)/(4|\nu|^2)$, $\xi = 0.01$ and $x_t = 47 + 0.1i$. μ_a is the critical value for having an absolute local instability. With our choice for μ_0, one single mode is unstable.

2.2 Discrete model

Equation (1) is discretized by a pseudo-spectral method using $N_x = 100$ Chebyshev polynomials (Trefethen, 2000; Boyd, 2001). The mapping $x = \frac{\ell}{2}\left(1 - \frac{1}{\alpha}\tan\left(\lambda\, x_{\text{Cheb}}\right)\right)$ (Bayliss and Turkel, 1992), with $\lambda = \arctan(\alpha)$ and $\alpha = 1$, is applied for obtaining a mesh of collocation points defined in Γ with a good discretization in the middle of the domain. Dirichlet and Neumann boundary conditions are enforced by Lagrange multipliers. A BDF2 implicit scheme is used for time discretization, with a time step $\Delta t = 0.05$.

After discretization, we obtain the system

$$\begin{cases} \begin{pmatrix} \mathbb{I} & 0 \\ 0 & 0 \end{pmatrix} \dfrac{\mathrm{d}}{\mathrm{d}t} \begin{pmatrix} \boldsymbol{z}_h \\ \boldsymbol{\lambda} \end{pmatrix} = \begin{pmatrix} A_{11} & A_{21}^* \\ A_{21} & 0 \end{pmatrix} \begin{pmatrix} \boldsymbol{z}_h \\ \boldsymbol{\lambda} \end{pmatrix} + \begin{pmatrix} B_1 \\ B_2 \end{pmatrix} \boldsymbol{c} + \begin{pmatrix} F_1 \\ F_2 \end{pmatrix} \boldsymbol{f}. \\ \boldsymbol{y} = H\boldsymbol{z}_h + \boldsymbol{r}, \end{cases} \tag{2a}$$

with the state values at the collocation points $\boldsymbol{z}_h$, the control $\boldsymbol{c}$, the measurements $\boldsymbol{y}$, the state perturbation $\boldsymbol{f}$ and the measurement perturbation $\boldsymbol{r}$. The constraints expressed in the second line of equation (**??**) describe the Dirichlet and Neumann boundary conditions and $\boldsymbol{\lambda}$ is the associated Lagrange multiplier. To eliminate the Lagrange multiplier, we define the projector $\Pi = \mathbb{I} - A_{21}^*(A_{21}A_{21}^*)^{-1}A_{21}$ as in Heinkenschloss et al. (2008), with $\Pi^* = \Pi$; and we split the discretized state $\boldsymbol{z}_h = \Pi\boldsymbol{z}_h + (\mathbb{I} - \Pi)\boldsymbol{z}_h$. Defining

$\boldsymbol{z} = \Pi \boldsymbol{z}_h$, we obtain the projected system

$$\begin{cases} \dfrac{\mathrm{d}\boldsymbol{z}}{\mathrm{d}t} = A\boldsymbol{z} + B\boldsymbol{c} + F\boldsymbol{f}. \\ \boldsymbol{y} = H\boldsymbol{z} + D\boldsymbol{c} + \boldsymbol{r}, \end{cases} \tag{3}$$

with

$$\begin{aligned} &A = \Pi A_{11} \Pi, \quad D = -H A_{21}^* (A_{21} A_{21}^*)^{-1} B_2, \\ &B = \Pi B_1 - \Pi A_{11} A_{21}^* (A_{21} A_{21}^*)^{-1} B_2, \\ &F = \Pi F_1 - \Pi A_{11} A_{21}^* (A_{21} A_{21}^*)^{-1} F_2, \end{aligned} \tag{4}$$

and the remaining part $(\mathbb{I} - \Pi)\boldsymbol{z}_h = -A_{21}^* (A_{21} A_{21}^*)^{-1} B_2 \boldsymbol{c}$.

2.3 Reduced system

The robust control approach has to be based on a low-dimensional model for making the design and the implementation feasible. We then split the linear system under observation into a stable part and an unstable part. The system (3) can be split as follows

$$\begin{cases} \dfrac{\mathrm{d}\boldsymbol{z}_u}{\mathrm{d}t} = A_u \boldsymbol{z}_u + B_u \boldsymbol{c} + F_u \boldsymbol{f} \\ \dfrac{\mathrm{d}\boldsymbol{z}_s}{\mathrm{d}t} = A_s \boldsymbol{z}_s + B_s \boldsymbol{c} + F_s \boldsymbol{f} \\ \boldsymbol{y} = H_u \boldsymbol{z}_u + H_s \boldsymbol{z}_s + D\boldsymbol{c} + \boldsymbol{r}, \end{cases} \tag{5}$$

with $\boldsymbol{z} = \Phi_u \boldsymbol{z}_u + \Phi_s \boldsymbol{z}_s$, such that the unstable part $\boldsymbol{z}_u$ is of small dimension n_u and that the component $\boldsymbol{z}_s$, of large dimension n_s, is stable. The columns of the matrices Φ_u and Φ_s are the direct unstable and stable eigenmodes respectively. We obtain

$$\begin{aligned} &A_u = (\Psi_u, A\Phi_u),\ A_s = (\Psi_s, A\Phi_s),\ B_u = (\Psi_u, B), \\ &B_s = (\Psi_s, B),\ F_u = (\Psi_u, F),\ F_s = (\Psi_s, F), \\ &H_u = H\Phi_u,\ H_s = H\Phi_s, \end{aligned} \tag{6}$$

where the columns of the matrices Ψ_u and Ψ_s are the adjoint eigenmodes. The inner-product $(x, y) = x^* W y$, is defined by W, the diagonal matrix containing the quadrature coefficients associated with the discretization. In the unstable system, we keep all unstable modes and eventually in addition a finite number of stable modes appropriately chosen. In section 3 only unstable modes are kept, and we will discuss in section 4 the performance improvement when additional stable modes are involved in the component $\boldsymbol{z}_u$.

Using the splitting (5), the measurement can be rewritten as

$$\boldsymbol{y} = H_u \boldsymbol{z}_u + H_s \boldsymbol{z}_s + D\boldsymbol{c} + \boldsymbol{r}. \tag{7}$$

Concerning the control, we search for a linear control law depending only on the estimated unstable state $\hat{\boldsymbol{z}}_u$, *i.e.* $\boldsymbol{c} = K\hat{\boldsymbol{z}}_u$, where K is the feedback gain. For consistency with (7), we would like to define the

estimated system incorporating $H_s\hat{\boldsymbol{z}}_s$ in the Kalman filter as follows

$$\begin{cases} \dfrac{\mathrm{d}\hat{\boldsymbol{z}}_u}{\mathrm{d}t} = \widetilde{A}_u\hat{\boldsymbol{z}}_u + B_uK\hat{\boldsymbol{z}}_u + L\left((H_u+DK)\hat{\boldsymbol{z}}_u + H_s\hat{\boldsymbol{z}}_s - \boldsymbol{y}\right) \\ \dfrac{\mathrm{d}\hat{\boldsymbol{z}}_s}{\mathrm{d}t} = A_s\hat{\boldsymbol{z}}_s + B_sK\hat{\boldsymbol{z}}_u, \end{cases} \tag{8}$$

with $\widetilde{A}_u = \left(A_u + \frac{1}{\gamma^2}F_uQ_eF_u^*X_u\right)$ and γ the robustness parameter. In the estimation, we consider that the unstable system is submitted to the worst perturbation. Q_e is the covariance matrix of the modeling noise, X_u is the solution of the Riccati equation defined later in (11) and L is the searched Kalman gain.

The estimated state $\hat{\boldsymbol{z}}_s$ is of high dimension, and classically, the associated dynamical system satisfied by $\boldsymbol{z}_s$ is projected onto an appropriate subspace. Here, we prefer to avoid this step. Let us notice that in (8), the estimator does not take into account the disturbance $F_s\boldsymbol{f}$ of system (5). Indeed, the observation can be written as

$$\boldsymbol{y} = H_u\boldsymbol{z}_u + H_se^{tA_s}\boldsymbol{z}_s(0) + \int_0^t H_se^{(t-\tau)A_s}B_sK\hat{\boldsymbol{z}}_u\,\mathrm{d}\tau + \int_0^t H_se^{(t-\tau)A_s}F_s\boldsymbol{f}\,\mathrm{d}\tau + D\boldsymbol{c} + \boldsymbol{r}, \tag{9}$$

and the estimator as

$$\begin{cases} \dfrac{\mathrm{d}\hat{\boldsymbol{z}}_u}{\mathrm{d}t} = \widetilde{A}_u\hat{\boldsymbol{z}}_u + B_uK\hat{\boldsymbol{z}}_u + L\left((H_u+DK)\hat{\boldsymbol{z}}_u + H_s\hat{\boldsymbol{z}}_s - \boldsymbol{y}\right) \\ H_s\hat{\boldsymbol{z}}_s = H_se^{tA_s}\boldsymbol{z}_s(0) + \displaystyle\int_0^t H_se^{(t-\tau)A_s}B_sK\hat{\boldsymbol{z}}_u(\tau)\,\mathrm{d}\tau. \end{cases} \tag{10}$$

The central piece of the formalism is that the effect of the full stable part is taken into account by the low-dimensional kernel $\mathcal{R}(t) = H_se^{tA_s}B_sK$. Projection onto an approximation subspace is then avoided. The response of the stable part to perturbations is omitted, but a finite number of stable modes can be freely incorporated to the unstable component for estimation enhancement.

In this paper, since the system is of moderate dimension, $\mathcal{R}(t)$ is computed explicitly. For large scale systems, it has to be computed as the impulse response of the stable system, taking as input actuators and output the measurements. This can be performed integrating in time the homogeneous linear system with $B - \Phi_uB_u$ as initial condition. By comparing the offline computational costs with other methods, it can be noted that BPOD requires impulse response of the direct and adjoint linear system, and that BT needs the resolution of a large scale Lyapunov equation, where A_s is not sparse.

3 Plant-compensator coupling

3.1 Gain computations

To determine the feedback and filtering gains (K, L), we use the standard $\mathcal{H}_\infty$ control theory (Doyle et al., 1989; Zhou et al., 1996). This leads to the resolution of the two Riccati equations:

$$\begin{cases} A_{u,\omega}^*X_u + X_uA_{u,\omega} - X_uM_uX_u + C_u^*C_u = 0 \\ A_uY_u + Y_uA_u^* - Y_uN_uY_u + F_uQ_eF_u^* = 0, \end{cases} \tag{11}$$

with $A_{u,\omega} = A_u + \Omega$, $M_u = \left(B_uR^{-1}B_u^* - \frac{1}{\gamma^2}F_uQ_eF_u^*\right)$ and $N_u = \left(H_u^*R_e^{-1}H_u - \frac{1}{\gamma^2}(C_u^*C_u + \Omega^*X_u + X_u\Omega)\right)$. We define the shift matrix $\Omega = \mathrm{diag}(\omega_1, \ldots, \omega_{n_u})$, where ω_i prescribes a decay rate of the mode i. In the design,

we have chosen to treat the unstable modes differently from the stable ones. If only the unstable modes are considered, we specify

$$A_{u,\omega} = A_u - \omega\mathbb{I} \quad , \quad C_u = 0, \tag{12}$$

that corresponds to a minimal energy control. If more stable modes are kept, we consider the matrices

$$A_{u,\omega} = A_u - \omega \begin{pmatrix} \mathbb{I} & 0 \\ 0 & 0 \end{pmatrix} \quad , \quad C_u = \begin{pmatrix} 0 & 0 \\ 0 & r\mathbb{I} \end{pmatrix}, \tag{13}$$

such that a constant shift ω is applied to all unstable modes. r is a parameter that specifies the control performances associated with the stable modes. Concerning the estimation, the noises are defined according to section 2.1, and then we have $R_e = \sigma_o^2\mathbb{I}$ and $Q_e = \sigma_f^2\mathbb{I}$. Finally, the gains are

$$K = -R^{-1}B_u^* X_u, \quad L = -\left(\mathbb{I} - \frac{1}{\gamma^2}X_u Y_u\right)^{-1} Y_u H_u^* R_e^{-1}. \tag{14}$$

3.2 Coupling

For evaluating the benefit of using the integral term $\int_0^t \mathcal{R}(t-\tau)\hat{\boldsymbol{z}}_u(\tau)\,\mathrm{d}\tau$ in the Kalman filter, we consider three compensated systems: The full information system that does not involve any estimation as a "best-case" reference, the partially coupled system that omits the integral term, and the fully coupled system that takes it into account.

Full information system First, the full information system allows us to have a comparison with a perfect estimation

$$\frac{\mathrm{d}\boldsymbol{z}}{\mathrm{d}t} = (A + BK)\boldsymbol{z} + F\boldsymbol{f}. \tag{15}$$

For model comparisons, we define generic notations of closed loop matrices, that are in the full information case $A_{\text{CL}} = A + BK$, $C_{\text{CL}} = C$, $H_{\text{CL}} = H$, $F_f = F$. The matrix C is chosen for an energy representation of the performance output $\|C\boldsymbol{z}\|^2 = \frac{1}{\ell}\int_0^\ell |\boldsymbol{z}|^2 \mathrm{d}x$. This leads to $C = \text{chol}(W/\ell)$ where $\text{chol}(\cdot)$ is the Cholesky factorization.

Partially coupled system (without integral term) Let us introduce the estimation errors $\boldsymbol{e}_u = \boldsymbol{z}_u - \hat{\boldsymbol{z}}_u$ and $\boldsymbol{e}_s = \boldsymbol{z}_s - \hat{\boldsymbol{z}}_s$. Control and estimation are classically coupled assuming that $\hat{\boldsymbol{z}}_s = 0$, that leads to the following system

$$\frac{\mathrm{d}}{\mathrm{d}t}\begin{pmatrix} \boldsymbol{z}_u \\ \boldsymbol{z}_s \\ \hline \boldsymbol{e}_u \end{pmatrix} = \underbrace{\left(\begin{array}{cc|c} A_u + B_u K & 0 & -B_u K \\ B_s K & A_s & -B_s K \\ \hline 0 & LH_s & \widetilde{A}_u + LH_u \end{array}\right)}_{A_{\text{CL}}} \begin{pmatrix} \boldsymbol{z}_u \\ \boldsymbol{z}_s \\ \hline \boldsymbol{e}_u \end{pmatrix} + \left(\begin{array}{cc} F_u & 0 \\ F_s & 0 \\ \hline F_u & L \end{array}\right) \begin{pmatrix} \boldsymbol{f} \\ \boldsymbol{r} \end{pmatrix}. \tag{16}$$

Even if $A_u + B_u K$ and $\widetilde{A}_u + LH_u$ are stable, stability cannot be guaranteed due to the off-diagonal term LH_s. We define in that case the closed loop matrices $C_{\text{CL}} = (C\Phi_u, C\Phi_s, 0)$, $H_{\text{CL}} = (H_u, H_s, 0)$, $F_f = (Fu; F_s; F_u)$, $F_o = (0; 0; L)$.

Fully coupled system (with integral term) The shape of system (8) is convenient as a basis to define the fully coupled system, that is transformed with the change of variable into

$$\frac{\mathrm{d}}{\mathrm{d}t}\begin{pmatrix}\boldsymbol{z}_u\\ \boldsymbol{z}_s\\ \hline \boldsymbol{e}_u\\ \boldsymbol{e}_s\end{pmatrix} = \underbrace{\left(\begin{array}{cc|cc} A_u+B_uK & 0 & -B_uK & 0\\ B_sK & A_s & -B_sK & 0\\ \hline 0 & 0 & \widetilde{A}_u+LH_u & LH_s\\ 0 & 0 & 0 & A_s\end{array}\right)}_{A_{\mathrm{CL}}}\begin{pmatrix}\boldsymbol{z}_u\\ \boldsymbol{z}_s\\ \hline \boldsymbol{e}_u\\ \boldsymbol{e}_s\end{pmatrix}\left(\begin{array}{cc} F_u & 0\\ F_s & 0\\ \hline F_u & L\\ F_s & 0\end{array}\right)\begin{pmatrix}\boldsymbol{f}\\ \boldsymbol{r}\end{pmatrix}. \tag{17}$$

Written like this, it can be seen that due to the block diagonal structure, the stability is guaranteed provided that $A_u + B_uK$ and $\widetilde{A}_u + LH_u$ are stable. We take here implicitly into account the term $H_s\hat{\boldsymbol{z}}_s = H_s e^{tA_s}\boldsymbol{z}_s(0) + \int_0^t H_s e^{(t-\tau)A_s}B_sK\hat{\boldsymbol{z}}_u\,\mathrm{d}\tau$ in the Kalman filter. In that case, we define the closed loop matrices as $C_{\mathrm{CL}} = (C\Phi_u, C\Phi_s, 0, 0)$, $H_{\mathrm{CL}} = (H_u, H_s, 0, 0)$, $F_f = (Fu; F_s; F_u; F_s)$, $F_o = (0; 0; L; 0)$.

Transfer functions and pseudospectra For comparisons between the control laws, we consider the system submitted to a perturbation forcing. We then define the transfer function between the model perturbation $\boldsymbol{f}$ and the output $C\boldsymbol{z}$ as the maximum Hankel singular values of the resolvent operator with appropriate input-output matrices

$$T_{\boldsymbol{f}\to\boldsymbol{z}}(\lambda) = \sigma_{\max}\left(C_{\mathrm{CL}}\left(A_{\mathrm{CL}} - \lambda\mathbb{I}\right)^{-1}F_f\right). \tag{18}$$

Moreover, ϵ-pseudospectra (Trefethen and Embree, 2005) are defined by domain in the complex plane such that $T_{\boldsymbol{f}\to\boldsymbol{z}}(\lambda) > \epsilon^{-1}$, with $\lambda = \lambda_r + i\lambda_i$.

3.3 Results

We first compare the three coupled systems in the case where only the unstable mode is incorporated in the unstable part. The parameter $\omega = 0.5\lambda_{r,1}$, with $\lambda_{r,1}$ the real part of the most unstable eigenvalue, has been selected as a trade off between the $\mathcal{H}_\infty$ performance $\|T_{\boldsymbol{f}\to\boldsymbol{z}}\|_\infty = \sup_{\lambda_i} T_{\boldsymbol{f}\to\boldsymbol{z}}(i\lambda_i)$ and the value of ω that induces large control amplitudes. Figure 1 compares spectra and ϵ-pseudospectra of the partially and fully coupled system, superimposed on the full information case. We first notice that taking into account the integral term, the spectrum of the fully coupled system (figure 1(b)) is very similar to that of the full information. In contrary, in the case of partial coupling (figure 1(a)), the spectrum is corrupted, and we recall that stability is not guaranteed. We can see in figure 1(b) that with the full coupling, even if the spectrum seems to be preserved, the transfer function is still modified, since the perturbation $\boldsymbol{f}$ acts differently in (17) and in (15).

In figure 2 the transfer functions $T_{\boldsymbol{f}\to\boldsymbol{z}}(i\lambda_i)$ along the imaginary axis of the three coupled systems are compared. We can see first that the $\mathcal{H}_\infty$ performance is degraded when estimation is considered compared to the full information situation. However, the full coupling slightly smooth out the peak, that improves the $\mathcal{H}_\infty$ performance compared to the partial coupling. Values of $\mathcal{H}_2$/$\mathcal{H}_\infty$ performances are reported in table 1.

For exploring more in detail the effect of the integral term on the estimation, a simulation of the closed loop systems submitted to a stochastic forcing $\boldsymbol{f}$ and a measurement noise $\boldsymbol{r}$ have been computed. The levels of the white noises are consistent with section 2.1. Figure 3(a) displays the instantaneous energy of

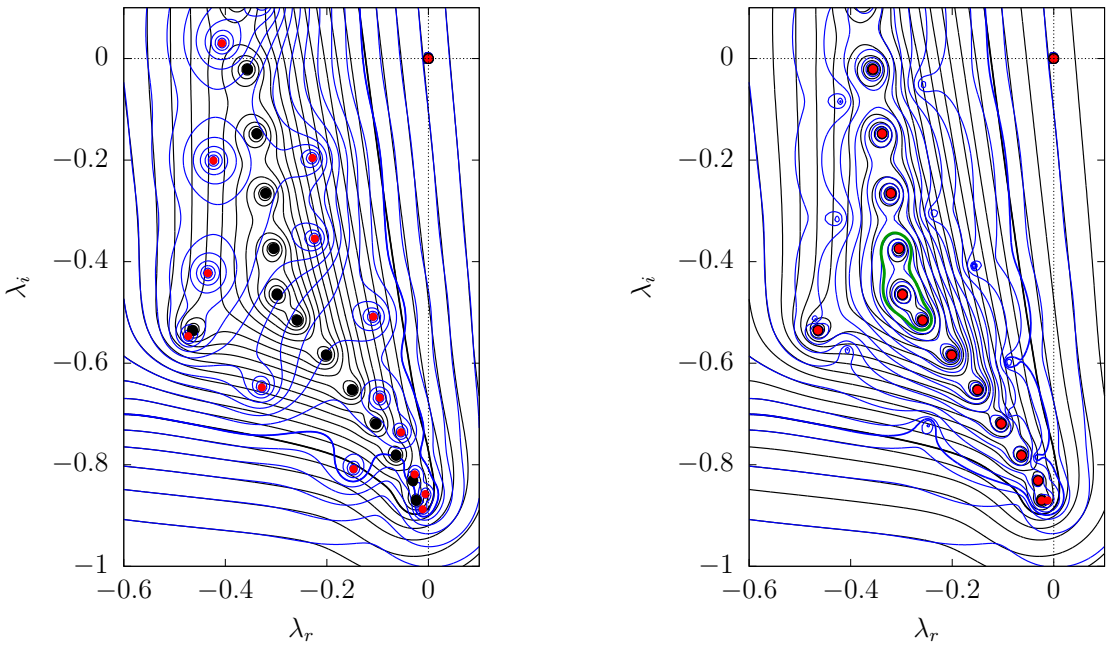

(a) Partial coupling.

(b) Full coupling.

Figure 1: Spectra and pseudospectra of the compensated systems keeping only the unstable mode. Lines are $\log_{10}(\sigma_{\max})$. Full information in black, coupled system in red dots (for eigenvalues) and blue lines (for pseudospectra). The thick line represents the unitary isocontour. Isolines have a spacing of 0.2, except isocontours of the fully coupled pseudospectrum (right) that are spaced of 0.4 for readability. Green line is an isocontour of $T_{\boldsymbol{f}\to\boldsymbol{z}}$ that circles the selected stable modes in section 4

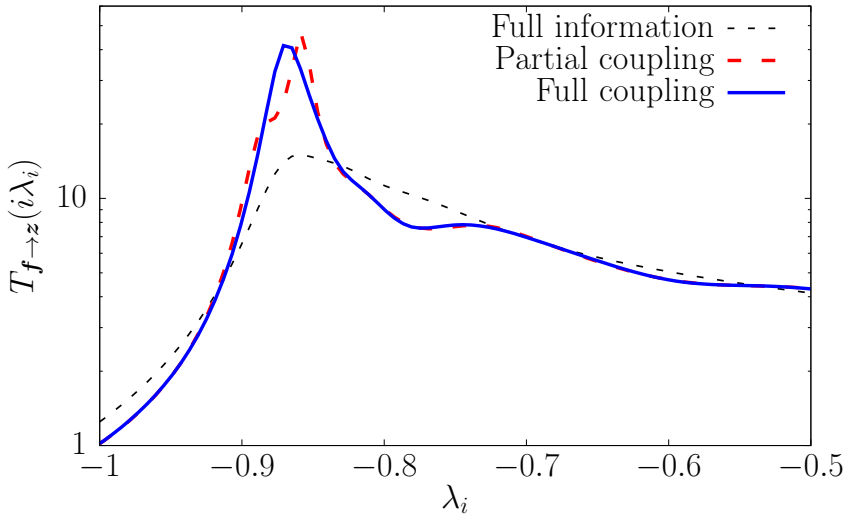

Figure 2: Transfer function $T_{\boldsymbol{f}\to\boldsymbol{z}}(i\lambda_i)$ along the imaginary axis of the compensated systems keeping only the unstable mode. Comparison between full information, partial coupling and full coupling.

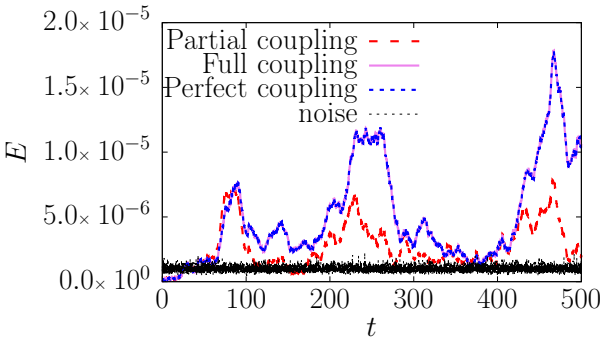

(a) Instantaneous energy. Noise level $\|C\boldsymbol{f}\|^2$ (black) and response $\|C\boldsymbol{z}(t)\|^2$ of the partially coupled system (dashed red), the fully coupled system (solid pink) and the perfectly coupled system (dashed blue).

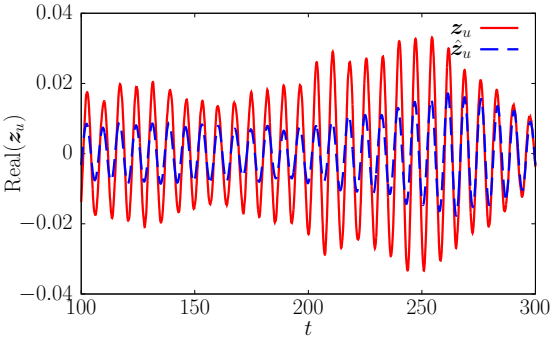

(b) Estimation of the unstable mode (dashed blue) compared with the state projection (solid red). Fully coupled system.

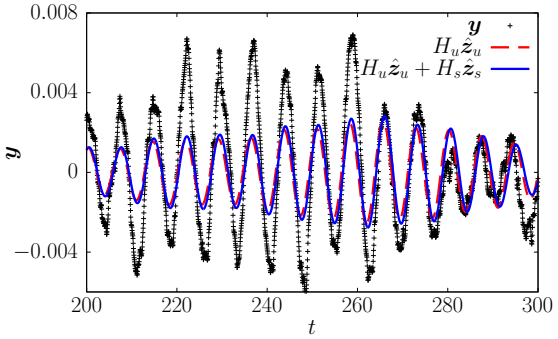

(c) Observation of the sensor at $x_{o1} = 47$ for fully coupled system. Comparison between measurement (black dot) with $H_u\hat{\boldsymbol{z}}_u$ (dashed red) and $H_u\hat{\boldsymbol{z}}_u + H_s\hat{\boldsymbol{z}}_s$ (solid blue).

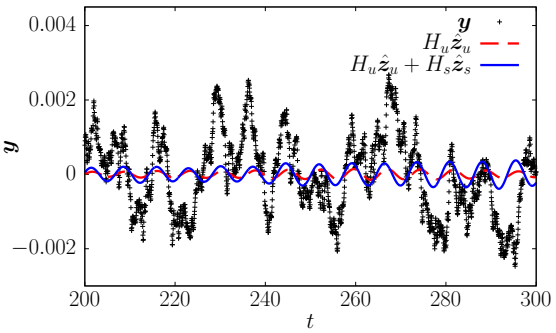

(d) Observation of the sensor at $x = 110$ for fully coupled system. Comparison between measurement (black dot) with $H_u\hat{\boldsymbol{z}}_u$ (dashed red) and $H_u\hat{\boldsymbol{z}}_u + H_s\hat{\boldsymbol{z}}_s$ (solid blue).

Figure 3: Estimation performances for partial and full coupling, when only the unstable mode is considered.

the solution, that reflects the $\mathcal{H}_2$ performance $\|T_{\boldsymbol{f}\to\boldsymbol{z}}\|_2 = \left(\int_{-\infty}^{+\infty} |T_{\boldsymbol{f}\to\boldsymbol{z}}(i\lambda_i)|^2 \,\mathrm{d}\lambda_i\right)^{\frac{1}{2}}$ (see for instance Levine, 1996). First of all for validation purpose, the simulation with the integral term (denoted fully coupled system) is compared with a simulation where the system (17) is explicitly assembled (denoted perfectly coupled system). The very close match confirms the ability of the procedure to represent the effect of the stable part. It can be seen that the fully coupled system has a worst $\mathcal{H}_2$ performance than the partially coupled system, that is consistent with figure 2 and table 1. The lack of performance improvement that we would expect adding the integral term can be explained by a poor estimation enhancement. The estimation of the unstable mode is plotted in figure 3(b) that shows a moderate estimation performance since the phase is captured, but the amplitude is underestimated. We will see that it will be clearly improved in section 4 when stable modes are added in the estimator. Estimated observations with and without modeling the stable part are compared with measurements at two sensor positions: at $x_{o1} = 47$ (figure 3(c)) whose contribution is dominated by the unstable mode and at $x = 110$ (figure 3(d)), middle of Γ_o, more representative of stable modes. Stable modes have indeed a spatial support located more downstream than the unstable mode. We can see that the downstream sensor at $x = 110$ is less well predicted, that is expected since only the unstable mode is explicitly taken into account in the estimator. These two figures show that the modeling of $H_s\boldsymbol{z}_s$ has a very slight effect, that can be explained by the fact that we have neglected the dominant contribution: the response of the stable part to perturbations.

In summary, the integral term allows to couple the compensator and the plant with good stability properties and with a slight robustness enhancement. This good behavior is the consequence of the consistency between the operators associated with the plant and the estimator. However with a single mode, we have neglected the response of the stable part to perturbations, that prevent us from getting estimation and $\mathcal{H}_2$ performance improvements.

4 Incorporation of stable modes

4.1 Mode's selection

Until now, only the unstable mode has been taken into account explicitly in the estimator. Now, we would like to determine which part of the stable subspace has to be chosen in order to improve the estimation and the robustness to external forcing perturbations. Modes that are selected in the stable space first have to be controllable and observable. This can be checked for each mode independently by computing the two quantities

$$d_j^c = \frac{B_j B_j^*}{-2\,\mathrm{real}(\lambda_j)} \quad ; \quad d_j^o = \frac{H_j^* H_j}{-2\,\mathrm{real}(\lambda_j)}, \tag{19}$$

where B_j and H_j, also called modal control/observation residuals (Bewley and Liu, 1998), are the projections of B and H respectively onto the mode j. λ_j is the associated eigenvalue. The geometrical average $(d_j^c d_j^o)^{\frac{1}{2}}$ corresponds to the criterion of mode's selection that appears for instance in Bagheri et al. (2009); Ehrenstein et al. (2011); Barbagallo et al. (2009, 2011). We have observed large values of controllability degree d_j^c located near the rupture of slope in the eigenspectrum $\lambda_r \approx -0.3$. This is associated with large sensitivity of these modes to external forcing perturbations. This high sensitivity near a branch junction has been observed in other studies, for instance in Bewley and Liu (1998). These modes are indeed involved in strong non-normality of the system that makes them highly sensitive to perturbations and responsible of large transient growth. We are interested in incorporating them in the estimator, since the response of the stable part to external perturbations is the missing piece. Since these modes play together, we choose to use the ϵ-pseudospectrum of the closed-loop full information system as a selection criterion. The green isocontour drawn in figure 1 defines a single domain including the selected eigenvalues. This criterion allows us to select modes, identified highly sensitive, that are active together by non-normal effects. By definition of the pseudo-spectrum, a perturbation operator with a norm smaller than ϵ will not be able to move the eigenvalues outside this isocontour. This justifies to keep all the modes included inside the ϵ-isocontour. Obviously, this criterion is not sufficient to completely avoid undesirable behavior due to the spectral truncation, and we rely on the integral term for modeling the remaining part involved in non-normal interference effects.

We have tested several truncation values ϵ leading to 1, 3 and 7 kept modes respectively. We have also tried to keep the least stable mode for comparison purpose. In table 1, we compare the $\mathcal{H}_2$ and $\mathcal{H}_\infty$ performances of the different models. The selection of 3 modes possesses the lowest $\mathcal{H}_\infty$ value and is thus our mode's selection (indicated by the green isocontour of $T_{\boldsymbol{f}\to\boldsymbol{z}}$ in figure 1(b)). The selection of 7 modes leads to similar, but slightly worst performances, while 1 mode is clearly worst. This corroborates the idea that these modes are linked by non-normality. We moreover obtain better performances using the ϵ-pseudospectrum selection than keeping the least stable ones. Finally, BT obtains the better $\mathcal{H}_2$ performance, but the worst $\mathcal{H}_\infty$, that indicates more likely the integral term strategy than BT for robustness purpose. We obtained comparable performances between 3 and 6 BT modes.

Model	$\mathcal{H}_2$	$\mathcal{H}_\infty$
No stable mode full information	3.8	14.9
No stable mode partial coupling	4.9	47.6
No stable mode full coupling	6.2	42.1
1 least stable mode full coupling	4.3	16.3
1 stable mode full coupling	4.5	19.4
3 stable modes full coupling	4.2	15.8
7 stable modes full coupling	4.1	16.7
3 BT modes	4.0	20.3

Table 1: $\mathcal{H}_2$ and $\mathcal{H}_\infty$ performances of the various compensated systems.

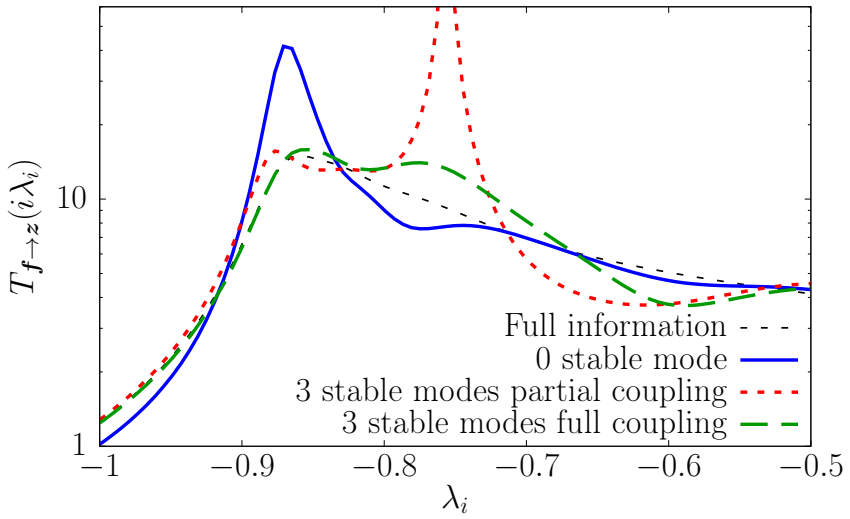

Figure 4: Transfer function $T_{\boldsymbol{f}\to\boldsymbol{z}}(i\lambda_i)$ along the imaginary axis of the compensated systems. Full information (short dashed black), fully coupled taking only the unstable mode into account (solid blue) and adding 3 stable modes (long dashed green). Partial coupling with 3 stable modes (dashed red).

4.2 Results

We have selected $r = 10^{-3}$ and $\gamma = 0.1$ such that $\|T_{\boldsymbol{f}\to\boldsymbol{z}}\|_\infty$ is minimal. Figure 4 shows the transfer function of the compensated system fully coupled, and we see that we have gained in $\mathcal{H}_\infty$ performance. The transfer function is closer to the full information transfer function, that suggests an estimation enhancement. Omitting the modeling of $H_s\boldsymbol{z}_s$ leads to a very large peak in the transfer function. In figure 5(a), numerical simulation, submitted to a stochastic forcing, confirms that we have gained in $\mathcal{H}_2$ performance as well. The estimation of $\boldsymbol{z}_u$ shown in figure 5(b) is clearly better than the one presented in section 3 figure 3(b). We can see as well how we improved the observation error in figures 5(c) and 5(d). The central point of the use of the integral term is illustrated in figure 5(d), where we see that $H_u\hat{\boldsymbol{z}}_u$ has a large norm, but adding $H_s\hat{\boldsymbol{z}}_s$ leads to an extremely accurate prediction of the downstream measurement at $x = 110$. This illustrates the interference effect between stable modes (that sign mainly at downstream positions), and the interest of modeling accurately the stable part by adding sensitive stable modes and use the integral term for compensating undesirable non-normal effects in the estimation.

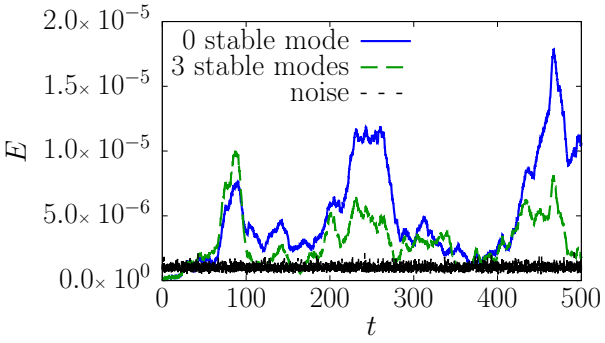

(a) Instantaneous energy. Noise level $\|C\boldsymbol{f}\|^2$ (black) and response $\|C\boldsymbol{z}(t)\|^2$ of the fully coupled system taking only the unstable mode into account (solid blue) and adding 3 stable modes (dashed green).

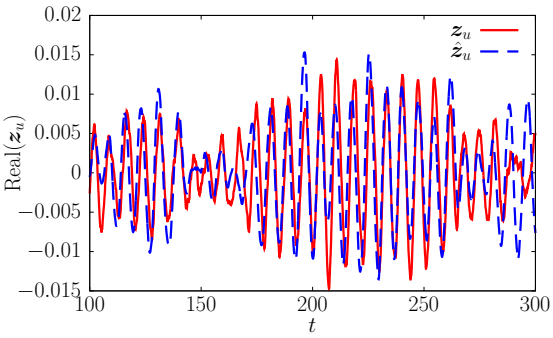

(b) Estimation of the unstable mode (dashed blue) compared with the state projection (solid red). Fully coupled system.

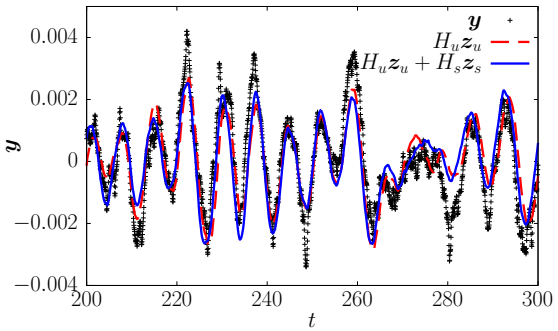

(c) Observation of the sensor at $x_{o1} = 47$ for fully coupled system. Comparison between measurement (black dot) with $H_u\hat{\boldsymbol{z}}_u$ (dashed red) and $H_u\hat{\boldsymbol{z}}_u + H_s\hat{\boldsymbol{z}}_s$ (solid blue).

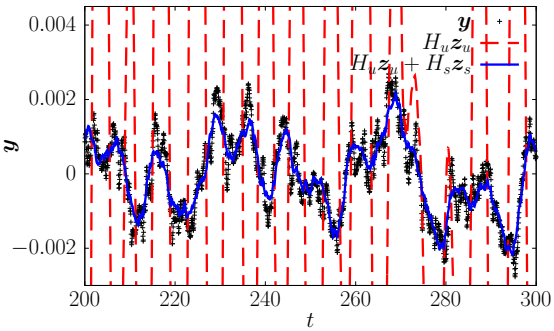

(d) Observation of the sensor at $x = 110$ for fully coupled system. Comparison between measurement (black dot) with $H_u\hat{\boldsymbol{z}}_u$ (dashed red) and $H_u\hat{\boldsymbol{z}}_u + H_s\hat{\boldsymbol{z}}_s$ (solid blue).

Figure 5: Estimation performances for full coupling when 3 stable modes are added.

5 Conclusion

In this paper, we have followed the strategy of using model reduction techniques based on global modes to derive a robust control with partial observations that guarantees the stability of the compensated system. For having consistency between estimated state and measurements, instead of performing an approximation of the stable part of the system by Galerkin projection, we have introduced an integral term in the Kalman filter that takes into account the response of the whole stable part to actuation through a precomputed kernel of low dimension. Numerical tests have demonstrated its benefits in terms of stability preservation and $\mathcal{H}_\infty$ performances. In a second step, we have shown that, properly selected, stable modes can be incorporated in the reduced-order model and can lead to drastic estimation improvements and to additional $\mathcal{H}_\infty/\mathcal{H}_2$ performances enhancements. We are currently adapting this strategy in the context of the feedback control of a flow over a thick plate, with boundary control and pressure measurements on the plate.

Acknowledments

This work was part of the CARPE project funded by RTRA STAE (Réseau Thématique de Recherche Avancée Sciences et Technologies pour l'Aéronautique et l'Espace).

References

A. C. Antoulas and D. C. Sorensen. Approximation of large-scale dynamical systems: An overview. *Applied Mathematics and Computer Science*, 11(5):1093–1122, 2001.

S. Bagheri, D. S. Henningson, J. Hœpffner, and P. J. Schmid. Input-output analysis and control design applied to a linear model of spatially developing flows. *Applied Mechanics Review*, 62(2), 2009.

A. Barbagallo, D. Sipp, and P. J. Schmid. Closed-loop control of an open cavity flow using reduced-order models. *Journal of Fluid Mechanics*, 641:1–50, 2009.

A. Barbagallo, D. Sipp, and P. J. Schmid. Input-output measures for model reduction and closed-loop control: application to global modes. *Journal of Fluid Mechanics*, 685:23–53, 9 2011. ISSN 1469-7645.

A. Bayliss and E. Turkel. Mappings and accuracy for Chebyshev pseudo-spectral approximations. *Journal of Computational Physics*, 101(2):349–359, 1992.

T. R. Bewley and S. Liu. Optimal and robust control and estimation of linear paths to transition. *Journal of Fluid Mechanics*, 365:305–349, 5 1998. ISSN 1469-7645.

J. P. Boyd. *Chebyshev and Fourier spectral methods*. Courier Dover Publications, 2001.

K. K. Chen and C. W. Rowley. $\mathcal{H}_2$ optimal actuator and sensor placement in the linearised complex Ginzburg–Landau system. *Journal of Fluid Mechanics*, 681:241–260, 7 2011. ISSN 1469-7645.

J. C. Doyle, K. Glover, P. P. Khargonekar, and B. A. Francis. State-space solutions to standard $\mathcal{H}_2$ and $\mathcal{H}_\infty$ control problems. *IEEE Transactions on Automatic control*, 34(8):831–847, 1989.

U. Ehrenstein, P. Y. Passaggia, and F. Gallaire. Control of a separated boundary layer: reduced-order modeling using global modes revisited. *Theoretical and Computational Fluid Dynamics*, 25(1):195–207, 2011.

M. Heinkenschloss, D. C. Sorensen, and K. Sun. Balanced truncation model reduction for a class of descriptor systems with application to the Oseen equations. *SIAM Journal on Scientific Computing*, 2008.

E. Lauga and T. R. Bewley. The decay of stabilizability with Reynolds number in a linear model of spatially developing flows. *Proceedings of the Royal Society of London. Series A: Mathematical, Physical and Engineering Sciences*, 459(2036):2077–2095, 2003.

W. S. Levine. *The control handbook*. CRC press, 1996.

J. L. Lumley. The structure of inhomogeneous turbulent flows. *Atmospheric turbulence and radio wave propagation*, pages 166–178, 1967.

J.-P. Raymond and L. Thevenet. Boundary feedback stabilization of the two dimensional navier-stokes equations with finite dimensional controllers. *Discrete and Continuous Dynamical Systems (DCDS-A)*, 27(3):1159–1187, 2010.

K. Roussopoulos and P. A. Monkewitz. Nonlinear modelling of vortex shedding control in cylinder wakes. *Physica D: Nonlinear Phenomena*, 97(1–3):264–273, 1996. ISSN 0167-2789.

C. W. Rowley. Model reduction for fluids, using balanced proper orthogonal decomposition. *International Journal of Bifurcation and Chaos*, 15(03):997–1013, 2005.

D. Sipp and P. J. Schmid. Linear closed-loop control of fluid instabilities and noise-induced perturbations: a review of approaches and tools. *Applied Mechanics Reviews*, 68(2):020801, 2016.

L. N. Trefethen. *Spectral methods in MATLAB*, volume 10. Siam, 2000.

L. N. Trefethen and M. Embree. *Spectra and pseudospectra: the behavior of nonnormal matrices and operators*. Princeton University Press, 2005.

K. Zhou, J. C. Doyle, K. Glover, et al. *Robust and optimal control*, volume 40. Prentice Hall New Jersey, 1996.